京都大学防災研究所年報 第 61 号 B 平成 30 年
DPRI Annuals, No. 61 B, 2018

A Transient Model for Shallow Groundwater Table Evolution in An Unconfined Sloping Aquifer Considering Variable Rainfall Recharge

Ying-Hsin WU and Eiichi NAKAKITA

Synopsis

This study presents a new numerical model for transient shallow groundwater table in an unconfined sloping aquifer considering rainfall recharge. The infiltration is neglected as only a thin sloping aquifer is considered. The theory for groundwater table evolution is the hydraulic groundwater theory, or called Dupuit-Boussinesq theory. The relaxation approach is applied for numerically calculating the nonlinear advection-diffusion equation with the help of the Godunov based finite volume scheme. The transient numerical model is verified with the steady-state solution. We performed two case studies considering variable rainfall patterns and variable aquifer hydraulic conductivity. The resultant hydrographs of outflow discharges and groundwater tables at the downstream outlet are obtained. The results verify that our transient model is practical for modelling motion of thin groundwater table in an unconfined sloping aquifer under variable rainfall patterns.

Keywords: groundwater table, unconfined aquifer, hillslope, numerical simulation, rainfall recharge, finite volume method

1 Introduction

In the recent decades, it is obvious that news of extreme or record-breaking rainfall having shorter durations and higher intensity becomes more frequent in many places around the world. Many researches have evidenced that global warming is one of important factors triggering this kind of extreme climate. Under this warming trend along with extreme rainfall, it is unavoidable to face more disasters we were not used to experience in the past, particularly in mountainous area. Extreme rainfall can alter stability condition of a hillslope. For correct prediction of shallow landslides, it is essential to better understand the response of groundwater in an aquifer under extreme rainfall. The groundwater motion is quite complicated in a hillslope aquifer having an unsaturated zone. In the unsaturated zone, water movement from hillslope surface to inner saturated zone is mainly controlled by infiltration process, which can be influenced by soil porosity property and capillary effect of partially saturated soil moisture. This process finally alters groundwater table evolution in the aquifer and corresponding seepage motion. In this study, we would like to focus on a thin aquifer having a characteristic length much greater than a characteristic depth under an extreme rainfall. Under this problem setting, the infiltration process is reasonably neglected in our analysis. Hence, the main purpose of this study aims to provide a new transient model for shallow groundwater table motion in a soil layer on hillslope surface under rainfall recharge without considering infiltration process.

Subsurface flow modelling has been investigated over several decades. For groundwater transport in the saturated zone in an aquifer, some hydrological models or theories have been proposed (e.g., Chow et al., 1988; Brutsaert, 2005; Lu and Jonathan, 2012). The famous Richards equation is the most conventional theory for subsurface flow modeling. The main

difficult of applying Richards equation is to obtain the free surface of groundwater, or says groundwater table, due to the nonlinear free-surface kinematic boundary condition (Bear, 1972). Also, for solving Richards equation the conventional numerical schemes are quite time-consuming, and are not appropriate to a wider calculation domain. However, for our target of a thin aquifer, this nonlinear difficulties can be overcome by applying the shallow flow approximation for equation simplification. The simplified theory is called the hydraulic groundwater theory, or called Dupuit-Boussinesq theory or Boussinesq theory for a short form (Brutsaert, 2005; Troch et al., 2013). For a sloping aquifer, some numerical models for Boussinesq theory have also been proposed (e.g., Stagnitti et al., 2004), but most models adopt either some further simplification or more restrictions on the theory. To our knowledge, none of numerical solution have been proposed for modelling using the original Boussinesq theory. Therefore, this work would like to overcome all past deficiencies to propose a new numerical approach for efficient and correct modelling of groundwater table evolution in a thin sloping aquifer on hillslope surface without involving infiltration.

The structure of this study goes as follows. The theoretical formulation is introduced in Section 2. The numerical scheme is stated in Section 3. Then, Section 4 introduces the settings of two case studies. Finally, the result and discussion are mentioned in Section 5, and conclusion is in Section 6.

2 Problem Formulation

We adopt a two-dimensional hillslope coordinate system, which x'-axis is aligned along and z'-axis is perpendicular to the slope surface, as is illustrated in Fig. 1. Generally, the depth, $\mathrm{O}(z') = H$, of soil layer mantling a natural hillslope is finite and thin comparing to the characteristic longitudinal length of a hillslope, $\mathrm{O}(x') = L$. Groundwater table and its variation in this thin soil layer can be considered to be thin and mild. This geometrical relation can give the shallow flow assumption,

$$\frac{H}{L} \ll 1. \tag{1}$$

In the field practices, the bottom of a soil layer mantling a hillslope usually consists of rock bed. As groundwater response in a thin layer is rapid and the time duration of our interest is only several hours, infiltration process is reasonably neglected in the soil layer as well as at the bottom bed rock boundary. Also, an unsaturated zone above groundwater table is too thin to be ignored.

2.1 Transient theory of groundwater table

With shallow flow assumption and Darcy's law for seepage motion, the transient equation of groundwater table evolution considering rainfall recharge can be expressed as (Brutsaert, 2005; Troch et al., 2013),

$$S_s \frac{\partial \eta'}{\partial t'} = k_0 \left[\cos\alpha \frac{\partial}{\partial x'} \left(\eta' \frac{\partial \eta'}{\partial x'} \right) + \sin\alpha \frac{\partial \eta'}{\partial x'} \right] + I', \tag{2}$$

where S_s is the specific yield [-], η' is the groundwater table [m], k_0 is the hydraulic conductivity [ms^{-1}], ranging from 10^{-1} to 10^{-5} m/s for general hillslopes, α is the slope inclination [°], I' is the rain rate [m/s] in the Cartesian z'-direction. The rain rate I' generally ranges from 10 to 200 mm/hr to represent from a slight to an extremely intense rainfall. In (2) the left-hand-side (LHS for abbreviation) denotes the time rate of groundwater table change, and the right-hand-side (RHS) denote mass in/out-flux and rainfall recharge terms, respectively. Then, the mass discharge can be expressed as

$$q' = \eta' u' = -k_0 \eta' \left(\cos\alpha \frac{d\eta'}{dx'} + \sin\alpha \right), \tag{3}$$

where the depth-averaging Darcy's seepage velocity reads

$$u' = -k_0 \left(\cos\alpha \frac{\partial \eta'}{\partial x'} + \sin\alpha \right), \tag{4}$$

where the minus sign means being positive in the right direction. A positive u' denotes a right-going flux in the positive x'-direction. Two boundary conditions are given at the downstream and upstream boundaries. A variable groundwater table is imposed at the downstream boundary $x' = 0$ as

$$\eta' = D(t). \tag{5}$$

Zero mass discharge is imposed at the upstream boundary $x' = L$, as below

$$q' = -k_0 \eta' \left(\cos\alpha \frac{d\eta'}{dx'} + \sin\alpha \right) = 0. \tag{6}$$

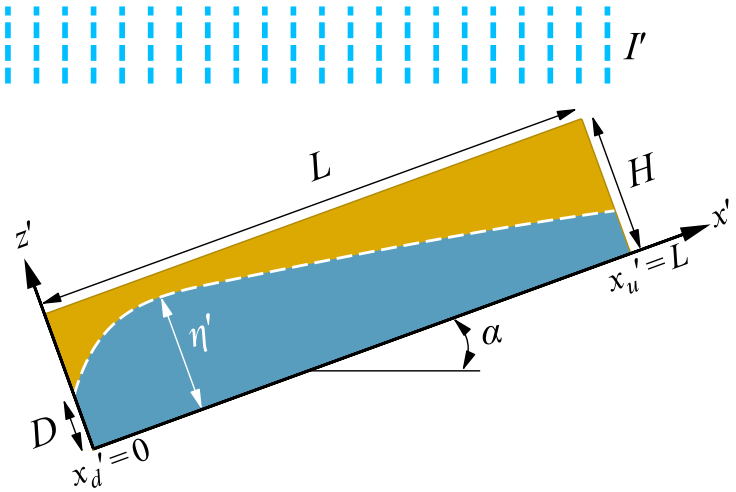

Figure 1: Geometry definition

Attention shall be paid to (6) that two possibilities for zero mass discharge exist. The way to impose an appropriate upstream boundary condition can refer to our previous work (Wu et al., 2018). Finally, an initial groundwater table is imposed as

$$\eta' = \eta'_0(x), \text{ at } t' = 0. \tag{7}$$

2.2 Normalization

All normalized variables are given as

$$x = \frac{x'}{L},\ \eta = \frac{\eta'}{H},\ u = \frac{u'}{\lambda},\ q = \frac{q'}{\lambda H},\\ t = \frac{t'}{S_s L/\lambda},\ \text{and } \lambda = \frac{k_0 H}{\cos\alpha L}. \tag{8}$$

Using (8), the governing equation (2) becomes

$$\frac{\partial \eta}{\partial t} = \frac{\partial}{\partial x}\left(\eta \frac{\partial \eta}{\partial x}\right) + \beta \frac{\partial \eta}{\partial x} + \gamma, \tag{9}$$

where

$$\beta = \frac{L\tan\alpha}{H} \quad \text{and} \quad \gamma = \frac{I' L^2}{k_0 H^2 \cos\alpha}, \tag{10}$$

Both of β and γ are positive parameters. β is called groundwater hillslope flow number (Brutsaert, 2005). A higher β represents flow in a shallower or steeper aquifer. Then, γ denotes the ratio of rain rate to hydraulic conductivity, and it represents the storage capacity of a aquifer during a rainfall recharge. A higher γ means a higher rainfall on an aquifer with lower permeability. Equation (9) is a nonlinear advection-diffusion equation having a variable diffusivity of η.

The normalized mass discharge reads

$$q = \eta u = -\eta\left(\frac{\partial \eta}{\partial x} + \beta\right), \tag{11}$$

where the normalized Darcy's seepage velocity reads

$$u = -\lambda\left(\frac{\partial \eta}{\partial x} + \beta\right). \tag{12}$$

The normalized downstream boundary condition becomes

$$\eta = \frac{D}{H} = \eta_0(t), \quad \text{at } x = 0. \tag{13}$$

At the upstream boundary, the normalized zero mass discharge becomes

$$q = -\eta\left(\frac{\partial \eta}{\partial x} + \beta\right) = 0, \text{ at } x = 1. \tag{14}$$

The normalized initial condition is

$$\eta = \eta_i(x), \text{ at } t = 0. \tag{15}$$

Some efforts have been made for theoretically analysing the transient problem with some approximations or linearization (e.g., Brutsaert, 2005; Troch et al., 2013). However, a technically-sound theoretical solution for the original transient Boussinesq theory has not been proposed yet. We adopt a reliable choice for verifying our numerical transient model with the steady state solution (Wu et al., 2018).

2.3 Steady state solution

The solution for the steady-state problem, which consists of (9) without the LHS term, has been revisited recently. Different downstream and upstream

boundary conditions can yield different groundwater table distributions. Particularly, at the upstream boundary, two boundary conditions exist under different given parameters, and appropriate boundary condition must be determined in advance for correct calculation. Recently an explicit formula has been proposed for determining appropriate upstream boundary conditions (Wu et al., 2018). Therefore, as the analytical steady state solution (Henderson and Wooding, 1964) is nonlinear and implicit, it still demands an iterative root-finding method for approximating the steady state solution. Instead of dealing with this implicit solution, we directly solve the equation of the steady state problem using conventional finite-difference method with an iterative algorithm and appropriate boundary conditions.

3 Numerical schemes

For our transient problem (9), the main concern for selecting an appropriate numerical scheme is that both of advection and nonlinear diffusion terms dominate. An explicit finite difference method is good for advection terms, but is quite time-consuming for diffusion term as a very small time step is demanded for numerical stability, or satisfying the Courant-Friedrichs-Lewy condition (abbreviated as CFL). Therefore, as a general practice, one usually suggests the popular Crank-Nicolson method, which is an implicit finite difference method having a fantastic advantage of unconditionally-stable property. However, in a steeper unconfined sloping aquifer, advection motion as well as some discontinuous groundwater table may exist in the groundwater flow. In this case, the Crank-Nicolson method is not applicable to a correct solution. Regarding this, in this study we shall utilize an alternative numerical scheme to precisely model groundwater table advection as well as diffusion processes.

To fit our numerical requirement, we shall adopt a Godunov-based finite volume scheme, which has intensely developed over past several decades, and is originally excellent at solving hyperbolic equations (LeVeque, 2002). Particularly, in the recent decades, some have proposed a new methodology, or called the relaxation approach, to hyperbolize parabolic equations into hyperbolic ones, and then to apply well developed Godunov schemes for precise numerical solutions (e.g., Nishikawa, 2014; Toro and Montecinos, 2014). Here, we shall apply this relaxation approach to solve our nonlinear transient problem (9).

3.1 Relaxation system

With some manipulations (LeVeque and Pelanti, 2001; LeVeque, 2002) to the original transient equation, the relaxation system is given as

$$\frac{\partial \eta}{\partial t} + \frac{\partial \psi}{\partial x} = \gamma, \tag{16}$$

$$\frac{\partial \psi}{\partial t} + d^2 \frac{\partial \eta}{\partial x} = -\frac{1}{\tau}\left(\psi + \eta\left(\frac{\partial \eta}{\partial x} + \beta\right)\right), \tag{17}$$

where τ is the relaxation time, and

$$\psi = -\eta\left(\frac{\partial \eta}{\partial x} + \beta\right) \text{ and } d = \left(\frac{\partial \eta}{\partial x} + \beta\right). \tag{18}$$

The eigenvalues or characteristic speeds of the system are readily obtained as

$$\lambda_{1,2} = \pm\left(\frac{\partial \eta}{\partial x} + \beta\right). \tag{19}$$

The key of the relaxation system is that by taking $\tau \to 0$ the RHS in (17) yields $\psi = -\eta(\frac{\partial \eta}{\partial x} + \beta)$, then (16) returns to the original transient system (9). For a stable approximation or preventing non-negative diffusion effect, the relaxation system need to satisfy a *sub-characteristic condition*,

$$-d_{\max} \le \frac{\partial \psi}{\partial \eta} \le d_{\max}, \tag{20}$$

where $d_{\max}$ is the maximum of d.

To solve the relaxation system, the relaxation scheme consists of two steps. The first is to update η^n to η^{n+1}(n denotes the numerical time step) by solving the hyperbolic system,

$$\frac{\partial}{\partial t}\begin{bmatrix}\eta \\ \psi\end{bmatrix} + \begin{bmatrix}0 & 1 \\ d^2 & 0\end{bmatrix}\frac{\partial}{\partial x}\begin{bmatrix}\eta \\ \psi\end{bmatrix} = \begin{bmatrix}\gamma \\ 0\end{bmatrix}. \tag{21}$$

The second step is to assign $\psi^{n+1} = \psi\left(\eta^{n+1}\right)$. Then, a Godunov-scheme applied in the first step is introduced in the following.

3.2 Wave propagation algorithm

Based on the upwind method and Godunov scheme, the wave propagation algorithm (LeVeque, 2002) is one of excellent methods for numerically solving hyperbolic problems and relaxation systems. By

adding correction fluxes, the high-resolution Godunov scheme of (21) in terms of wave propagation algorithm reads

$$\eta_i^{n+1} = \eta_i^n + \frac{\Delta t}{\Delta x}\left(\mathcal{A}^+\Delta\eta_{i-1/2}^n + \mathcal{A}^-\Delta\eta_{i+1/2}^n\right) + \frac{\Delta t}{\Delta x}\left(\tilde{F}_{i+1/2}^n - \tilde{F}_{i-1/2}^n\right), \tag{22}$$

where i is the cell index, Δx and Δt are spatial and temporal increments, $\mathcal{A}^+\Delta\eta_{i-1/2}^n$ and $\mathcal{A}^-\Delta\eta_{i+1/2}^n$ are the right-going and left-going fluxes from the left and right edges of the cell i, and $\tilde{F}_{i\pm1/2}^n$ are the second-order corrections for fluxes at the cell edges.

With a special treatment to the source term γ in (21) for satisfying well-balancing property, the flux decomposition at both edges of the cell i are expressed as

$$\left.\begin{aligned}\psi(\eta_i) - \psi(\eta_{i-1}) + \Delta x\bar{\Psi}_{i-1/2} &= \sum \mathcal{Z}_{i-1/2}^n \\ \psi(\eta_{i+1}) - \psi(\eta_i) + \Delta x\bar{\Psi}_{i+1/2} &= \sum \mathcal{Z}_{i+1/2}^n\end{aligned}\right\}, \tag{23}$$

where $\sum$ denotes the summation over the two waves propagating at $\lambda_{1,2}$, ψ refers to (18), and the gradient of η is discretized by the 2nd-order central difference,

$$\left.\frac{\partial\eta}{\partial x}\right|_i = \frac{\eta_{i+1} - \eta_{i-1}}{2\Delta x} \text{ at the cell } i, \tag{24}$$

$\mathcal{Z}_{i\pm1/2}^n$ denote the flux jumps at the left and right edges of the cell i, and $\bar{\Psi}_{i\pm1/2}$ denote the variable rainfall recharge terms at the edges of the cell i,

$$\left.\begin{aligned}\bar{\Psi}_{i-1/2} &= -\tfrac{1}{2}(\gamma_i + \gamma_{i-1}) \\ \bar{\Psi}_{i+1/2} &= -\tfrac{1}{2}(\gamma_{i+1} + \gamma_i)\end{aligned}\right\}, \tag{25}$$

In (22) the corrected fluxes $\tilde{F}_{i\pm1/2}^n$ at the cell i's edges are expressed as

$$\tilde{F}_{i\pm1/2}^n = \tfrac{1}{2}\times \sum \operatorname{sgn}\left(s_{i\pm1/2}^+\right)\left(1 - \frac{\Delta t}{\Delta x}|s_{i\pm1/2}^+|\right)\tilde{\mathcal{Z}}_{i\pm1/2}^n, \tag{26}$$

where $\operatorname{sgn}(\cdot)$ is the sign function, and the characteristic speeds at the left and right edges of the cell i read

$$\left.\begin{aligned}s_{i-1/2}^+ &= \max(0, s_i) \\ s_{i+1/2}^- &= \min(0, s_i)\end{aligned}\right\}, \tag{27}$$

in which the characteristic speed at the cell i is $s_i = \lambda_{1,2}$, and $\max(\cdot)$ and $\min(\cdot)$ are the functions for taking maximum and minimum values. Also, in (26) $\tilde{\mathcal{Z}}_{i\pm1/2}^n = \phi(\theta_{i\pm1/2}^n)\mathcal{Z}_{i\pm1/2}^n$ are limited waves using a total variation diminishing flux limiter ϕ, evaluated by ratios of wave strength $\theta_{i\pm1/2}^n$ at $i \pm 1/2$,

$$\theta_{i+1/2}^n = \mathcal{Z}_{i+3/2}^n / \mathcal{Z}_{i+1/2}^n. \tag{28}$$

Then, for avoiding any non-physical oscillation in this study, the high-resolution correction adopts the monotonized central-difference limiter, or called MC-limiter (LeVeque, 2002), as below

$$\phi_{\text{MC}}(\theta) = \max(0, \min((1+\theta)/2, 2, 2\theta)). \tag{29}$$

where θ is the ratio at the cell edges, i.e., (28).

The free outflow boundary condition is implemented at both of the problem's boundaries.

Finally, for holding numerical stability, the CFL condition reads

$$\Delta t \le \min\left(\frac{\mathcal{C}_{\max}\Delta x}{\max|\lambda_1, \lambda_2|}, \frac{\mathcal{D}_{\max}\Delta x^2}{\max(\eta)}\right), \tag{30}$$

with the Courant number $\mathcal{C}_{\max} = 1$ being general for the wave propagation algorithm, and $\mathcal{D}_{\max} = 0.5$ in our scheme (Toro and Hidalgo, 2009).

3.3 Verification

As analytic transient solution of Boussinesq theory is not available now, we turn to focus on verifying long-time simulation results of our transient numerical model. For verification, we used steady state solutions to compare with long-time numerical solutions. The test case is a rectangular aquifer having the dimension of 10 m long by 1 m high. This aquifer's inclination is 45°, and the downstream outlet is located in the left-end side. The hydraulic conductivity is set to be 1.0×10^{-4} m/s, the rain rate is $I = 216.0$ mm/hr, and the specific yield is $S_s = 0.4$ in the transient model. The simulation time is 500 minutes for the transient model. From Fig. 2 the groundwater table at $x = 0$ approaches a steady condition of $\eta_0 = 0.637$ m as time goes to 500 minutes. Then, the simulated groundwater table distribution of our transient model coincides well with the one of the steady state solution, as is shown in Fig. 3.

In addition, in Fig. 2 the discharge at the downstream outlet $x = 0$ can also be verified with an analytic formula. Applying our case's parameters to the analytic formula (Wu et al., 2018), the dimensional discharge is calculated as

$$q(x = 0) = -I'L\cos\alpha \approx -4.306 \times 10^{-4} \text{ cms}.$$

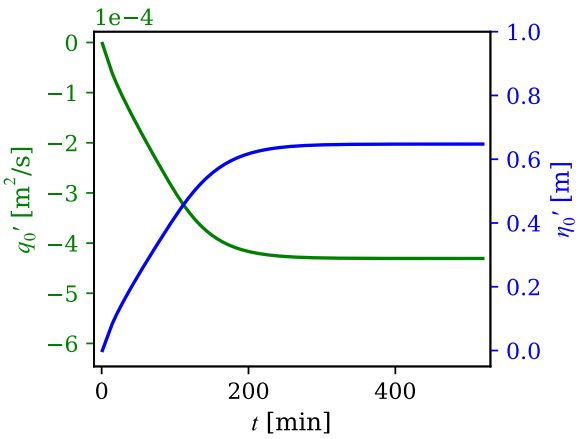

Figure 2: Hydrographs of mass discharge and groundwater table at the downstream outlet. The final values are $q_0 = -4.236 \times 10^{-4}$ m^2/s and $\eta_0 = 0.637$ m.

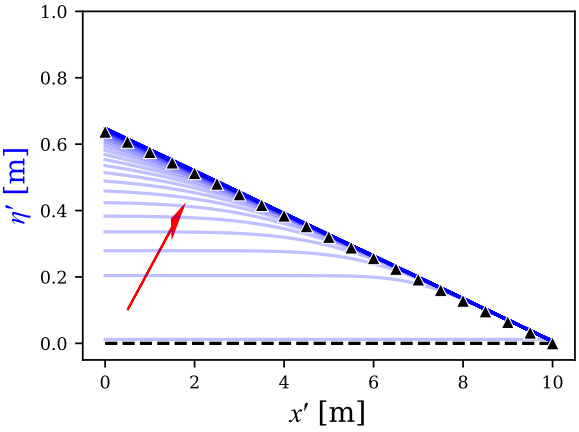

Figure 3: Verification using steady state solution (black triangles) under zero initial groundwater table (black dash line), $k_0 = 1.0 \times 10^{-3}$ m/s, $I = 216.0$ mm/hr, $\alpha = 45°$. Transparent blue lines denote transient model results. The red arrow denotes the change direction of groundwater table.

(31)

Comparing with the numerical result of $q = -4.243 \times 10^{-4}$ cms, the relative error is only about 1.5%. This also verifies our numerical model for long-time simulation. However, to put again, the initial-time simulation still requires further verification, but it may not be available now as having no appropriate analytic solutions so far.

4 Case study

To consider the hillslope aquifer response under extreme rainfall, we performed two artificial case studies of variable artificial rainfall patterns as well as variable aquifer hydraulic conductivity. We setup a rectangular aquifer having the same dimension of 10 m long by 1 m high. This aquifer's inclination is 30°, and the aquifer's left-end side is the downstream outlet. For representing an extreme rainfall, the peak value of rain rate is $I = 200$ mm/hr. The aquifer material is assumed to be isotropic and homogeneous. The aquifer's specific yield is constant $S_s = 0.4$. An initial groundwater table is also given as

$$\eta_0(x) = \frac{\exp\left(-50(x-0.6)^2\right)}{10\sqrt{0.02\pi}}, \tag{32}$$

where $\exp(\cdot)$ is the exponential function.

Because rainfall recharge and aquifer permeability are the main factors influencing groundwater table motion, we here consider two cases, including the first is to show the effect of variable rainfall patterns on an aquifer having a constant hydraulic conductivity of 1.0×10^{-3} m/s, and the second is to reveal the effect of variable aquifer hydraulic conductivity under a uniform distribution rainfall pattern. Parameters of both cases are introduced in the following.

Table 1: Rainfall distributions

Distribution	Formulas $x \in [0, 1]$
a) no rainfall	$I(x) = 0$
b) uniform rainfall	$I(x) = I_P$
c) linear rainfall	$I(x) = I_P x$
d) quadratic rainfall	$I(x) = I_P - (x - \frac{1}{2})^2$

† I_P is the normalized peak value of rain rate.

4.1 Variable rainfall patterns

As are listed in Table 1, four types of rainfall distributions are assumed here. The peak value of rain rate holds a linear function decaying from 200 mm/hr initially to 0 mm/hr after 120 minutes, as is shown in Fig. 4. Particularly, the linear rainfall distribution gives a maximum at the upstream, and linearly decreases to zero at the downstream. The quadratic rainfall pattern has a maximum at the aquifer middle, $x = 0.5$, but zeros at the upstream and downstream boundaries.

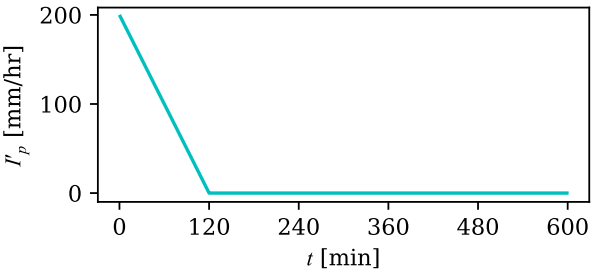

Figure 4: Decaying function of peak rain rate I'_P. Before 120 minutes it holds a linear decreasing rate, and after 120 minutes no rainfall exists.

4.2 Variable aquifer hydraulic conductivity

To reveal the effect of different soil composition, we consider four different aquifer hydraulic conductivity in different order of magnitudes, i.e., e) 1.0×10^{-1} m/s, f) 1.0×10^{-2} m/s, g) 1.0×10^{-3} m/s, and h) 1.0×10^{-4} m/s. For the sake of simplicity, only the uniform rainfall pattern is adopted here with the same decaying function in Fig. 4.

5 Results and Discussion

5.1 Variable rainfall patterns

Figure 5 illustrates hydrographs of discharge and groundwater table at the downstream outlet. As shown in Fig. 5a, without any rainfall recharge, the groundwater from the given initial groundwater table (32) starts to drain at the downstream outlet at about 65 minutes, and reaches a maximum groundwater table of 0.2 m and a maximum discharge of -1.0×10^{-4} cms at 134.5 min, and all groundwater finally drains out. In the other cases of uniform, linear, and quadratic rainfall patterns (please see Fig. 5b, c, and d), the maximum downstream discharge takes place in the case of uniform rainfall pattern at the value of 2.15×10^{-4} cms at 116.4 min, and the maximum groundwater table also happens in the same pattern at the depth of 0.424 m at around 132.4 min. This result is not surprised because the uniform rainfall pattern contributes the highest rainfall recharge to the sloping aquifer. This case testifies that our transient numerical model can successfully simulate groundwater table evolution with or without variable rainfall recharge.

5.2 Variable hydraulic conductivity

Not only rainfall patterns but aquifer material property also dominates groundwater flow. Figure 6 illustrates simulated hydrographs of discharge and groundwater table at the downstream outlet. Obviously, the higher hydraulic conductivity the aquifer soil possesses, the rapid the aquifer response takes place. For the highest $k_0 = 10^{-1}$ m/s (Fig. 6e), the maximum discharge and groundwater table happen at around 1.3 min in the values of -0.01 cms and 0.21 m, respectively. On the other hand, for the case of lowest hydraulic conductivity (Fig. 6h) the aquifer response can last for over 3,000 minutes in a rather smaller maximum discharge of 2.1×10^{-5} cms but a higher groundwater table of 0.404 m. The results verify that our numerical model can properly reveal the groundwater hysteresis.

6 Concluding remarks

We present a new transient model for numerically modelling shallow groundwater table evolution in an unconfined sloping aquifer under variable rainfall recharge without considering infiltration. The relaxation scheme with the wave-propagation algorithm is testified to be practical for numerical solutions. Two case studies have been performed for revealing the capability of our numerical model on modelling cases under variable conditions as well as on capturing the groundwater hysteresis effect. An additional merit of this work is that the Godunov-based relaxation scheme we applied can be easily extended to three dimensions. So, developing a three-dimensional transient model for groundwater table evolution would be our next target.

Acknowledgements

The authors appreciate the financial supports of Grant-in-aid for Japan Society for the Promotion of Science (JSPS) Fellows (Grant No.16F16378) and JSPS Postdoctoral Fellowship for Overseas Researchers for Y.H.W.

References

Bear, J. (1972): Dynamics of Fluids in Porous Media, Dover.

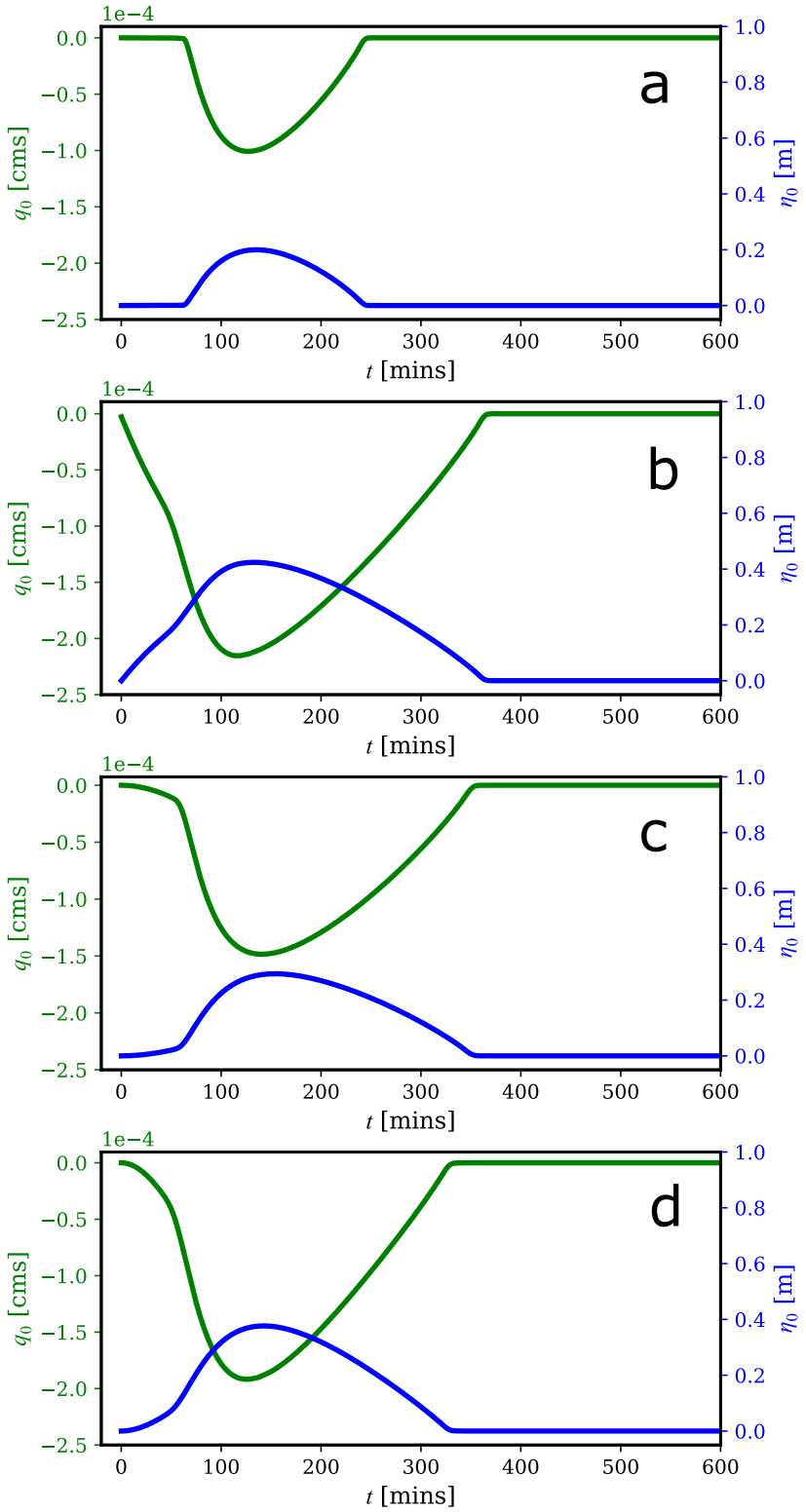

Figure 5: Hydrographs of simulated discharge (green line) and groundwater table (blue line) at the downstream outlet under variable rainfall patterns: a) no rainfall, b) uniform, c) linear, and d) quadratic rainfall patterns

Brutsaert, W. (2005): Hydrology, An Introduction, Cambridge University Press.

Chow, V.T., Maidment, D.R. and Mays, L.W. (1988): Applied Hydrology, McGraw-Hill.

Henderson, F.M. and Wooding, R.A. (1964): Overland flow and groundwater flow from a steady rainfall of finite duration, J. Geophys. Res., Vol. 69, No. 8, pp. 1531-1540.

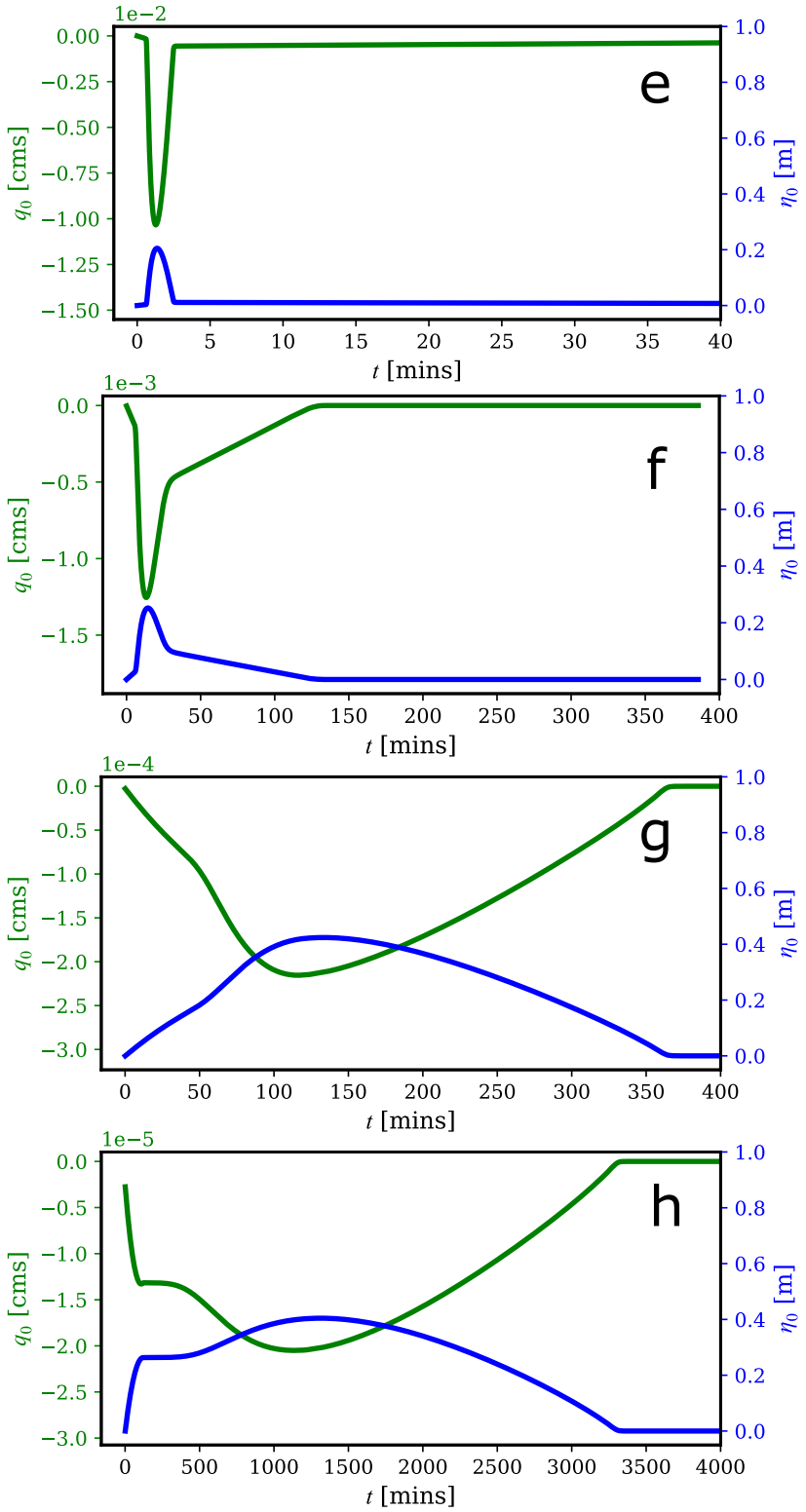

Figure 6: Hydrographs of simulated discharge (green line) and groundwater table (blue line) at the downstream outlet under uniform rainfall but variable hydraulic conductivity: e) 10^{-1}, f) 10^{-2}, g) 10^{-3}, and h) 10^{-4} m/s. The order of magnitude of x-axis and y-axis in each figure are different.

LeVeque, R.J. (2002): Finite Volume Methods for Hyperbolic Problems, Cambridge University Press.

LeVeque, R.J. and Pelanti, M. (2001): A class of approximate Riemann solvers and their relation to relaxation schemes, J. Comput. Phys., Vol. 172, pp. 572-591.

Lu, N. and Godt, J.W. (2012): Hillslope Hydrology and Stability, Cambridge University Press.

Nishikawa, H. (2014): First-, second-, and third-order finite-volume schemes for diffusion, J. Comput. Phys., Vol. 256, pp. 791-805.

Stagnitti F., et al. (2004): Drying front in a sloping aquifer: Nonlinear effects, Water Resour. Res., Vol. 40, W04601.

Toro, E.F. and Hidalgo, A. (2009): ADER finite volume shcemes for nonlinear reaction-diffusion equations, Appl. Numer. Math., Vol. 59, pp. 73-100.

Toro, E.F. and Montecinos, G.I. (2014): Advection-diffusion-reaction equations: hyperbolization and high-order ADER discretizations, SIAM J. Sci. Comput., Vol. 36, No. 5, pp. A2423-A2457.

Troch, P.A., et al. (2013): The importance of hydraulic groundwater theory in catchment hydrology: The legacy of Wilfried Brutsaert and Jean-Yves Parlange, Water Resour. Res., Vol. 49, pp. 5099-5166.

Wu, Y.-H., Sayama, T. and Nakakita, E. (2018): Appropriate boundary condition for Dupuit-Boussinesq theory on the steady groundwater flow in an unconfined sloping aquifer with uniform recharge, Water Resour. Res., doi:10.1029/2018WR023070.

(Received June 13, 2018)